Fibers and Polymers 2019, Vol.20, No.1, 165-176
DOI 10.1007/s12221-019-8575-y

ISSN 1229-9197 (print version)
ISSN 1875-0052 (electronic version)

Influence of Crosslinking Density on Antioxidant Nanocellulose in Bio-degradation and Mechanical Properties of Nitrile Rubber Composites

Mohamad Nurul Azman Mohammad Taib, Wageeh A. Yehye, and Nurhidayatullaili Muhd Julkapli*

Nanotechnology & Catalysis Research Centre (NANOCAT), Institute of Postgraduate Studies (IPS), University of Malaya, Kuala Lumpur 50603, Malaysia

(Received July 2, 2018; Revised October 9, 2018; Accepted October 22, 2018)

Abstract: Nanocellulose antioxidant (Aox-NCC) was used as reinforcement and crosslinking agent in nitrile butadiene rubber (NBR) composites. The crosslinking density and volume of rubber bonded in the matrix were increased up to 3 phr and no significant improvement between 4 phr and 5 phr was recorded. The interactions of gallic acid and NCC was found to occur between the -OH and -COOH groups, as revealed by Fourier Transform Infra-Red (FTIR) and Nuclear Magnetic Resonance (NMR) analysis. Crystallinity index of Aox-NCC was increased more than 11 %, recorded by X-ray diffraction (XRD) analysis. Meanwhile, the thermal stability of Aox-NCC was increased 30 °C, analyzed by thermogravimetry (TG). With the addition of 3 phr Aox-NCC, tensile strength and modulus at 500 % for NBR composites were increased significantly up to 20 %. There was no significant improvement on modulus at 100 %, modulus at 300 %, elongation at break and tear strength. The degradability of NBR composites within 6 months period was improved significantly at 5 phr of Aox-NCC. Increase in carbonyl group after soil burial test with the existence of cracks, voids and degradable parts of NBR composites were revealed. This demonstrated that, Aox-NCC plays a secure function to reinforce NBR composites.

Keywords: Cellulose, Nanocrystals, Biodegradable, Composites, Morphology

Introduction

Cellulose is one of the most abundance bio-polymer in nature building up from a linear syndiotactic homopolymer of β-(1-4)-glycosidic bonds linked D-anhydroclucopyranose [1,2]. Cellulose has a great advantage in terms of degradability and mechanical performance, as compared to other reinforced materials. The bending strength and modulus of cellulose in nanofibrils form are estimated to be 10 GPa and 150 GPa, respectively [1]. Nanocrystalline cellulose (NCC) with a diameter from 2 nm to 20 nm and length range from 100 nm to 2.1 um and are often called whiskers or nanowhiskers or nanofibrils and this can be produced, from many resources of natural fibres [3,4]. Despite the advantage, NCC has some drawbacks with a tendency to form agglomeration, due to hydrogen bonding and easily degrade in natural medium [1,5]. Thus, NCC has a limitation on a short lifespan and application to be used as a reinforcement material. Due to this, the combination of NCC with polymer matrix can improve the degradability element on the bio-polymer composites and create the environmentally friendly materials.

Latex, either natural or synthetic is the polymer, which is commonly used in the production of gloves. Latex is affected by degradation and ageing at the long-term exposure to oxygen, heat, light and ozone [6,7]. The resistance to latex degradation is due to the presence of effective antioxidant in latex compounds. Additional antioxidant element in latex, reduce the rate of polymer degradation [6]. Report by [8] indicates that, removal of antioxidants by organic solvents from latex, glove would increase the growth of rubber-bacteria degrading on latex. Chemical structure of and the cross bonding to composites components are the most significant factors, that contributes to the overall performance of antioxidant. Thus, addition of antioxidant into the latex compound is expected to prevent and slow down the degradation rate in the decomposition conditions [8]. The natural antioxidant that is added into the latex process is to minimize the harmful effects to the environment, when the degradation or decomposition process occurs. Thus, it would leach down the natural antioxidant into the environment during the decomposition process. This consequently prevent the soil from contamination of harmful chemicals. Natural antioxidant demonstrates a significant improvement on resistance of bio-materials. Natural antioxidant is commonly derived from the natural resources, available as a natural component and tolerance in most natural environmental conditions.

Production and demand for gloves are annual increased with demand from healthcare, food and other industries [9,10]. Many of research works have been conducted to find a solution to improve on this material, in terms of mechanical and physical properties. In addition, the lack of degradability properties of synthetic polymers have been come to most interest. Several researchers focusing on utilization of fillers or reinforcement materials to improve on mechanical properties with the addition of inorganic fillers, such as carbon black, silica, nanoclay, graphene and others [11-16]. Even though, addition of these reinforcements or fillers had improved the tensile strength and modulus of elongation. However, addition of inorganic filler supplied with several limitations. For example, the addition of graphene oxide and multi-wall carbon nanotube in manufacturing stage would

*Corresponding author: nurhidayatullaili@um.edu.my

cause to the time and cost constrain [17,18]. Furthermore, these fillers are inorganic and had created environmental issues.

Nitrile butadiene rubber (NBR) was derived from the petroleum resource and non-bio-degradable material. Disposable of this material by incineration or combustion method releases harmful and carcinogen chemicals such as, cyanide and hydrogen chloride Furthermore, the acetonitrile product of incomplete combustion of nitrile compounds, could enter the human bloodstream through inhalation and skin. The cyanide results in harmful to human in minimum doses [19].

In this study, new green nanocomposites that is based on nitrile butadiene rubber (NBR) is filled with antioxidant nanocellulose (Aox-NCC) was prepared. The Aox-NCC was characterized by FTIR, NMR, XRD, TGA, TEM and FESEM analyses before being incorporated into the NBR matrix. Furthermore, with varying weight percentage of Aox-NCCs in NBR matrix, the mechanical performance in tensile and tear strength, the biodegradability in the soil, chemical composition and surface morphology were investigated.

Experimental

Materials and Method

Cotton linter microcrystalline cellulose (MCC) with size 20 μm was bought from Friendemann Schmidt. Hydrochloric acid (HCl) 37 wt.% for hydrolysis, nitrile butadiene rubber (NBR) latex and ingredients were purchased from local supplier.

Synthesis of NCC

MCC (5 g) was added in 5 M of HCl concentration solution and the mixture was hydrolyzed at 100 °C for 60 minutes with continuous stirring (500 rpm), before it being quenched in ice to stop the reaction. The reaction mixture then was washed with distilled water before went for the centrifuge process (30 minutes at 3000 rpm; repeated configuration). The supernatant was removed from the sediment and replaced by raw distilled water and re-centrifuged for five times. The last wash was conducted using dialysis membrane with distilled water till reach to pH 7. The resultant suspension then was dried using freeze dryer to remove the moisture and eliminate the remaining water content in NCC before modification with antioxidant was done.

Preparation of Antioxidant NCC

The gallic acid antioxidant was added in 100 m*l* of water until saturated. NCC (1 g) was added into gallic acid solution with 2 days continuously stirring at room temperature. The beaker was sealed with parafilm. Then, the antioxidant NCC (Aox-NCC) was washed with distilled water for several times to stop the reaction, remove any residue and other by-product of treatment. The antioxidant NCC (Aox-NCC) was freeze dried for 2 hours.

Preparation of NBR/Aox-NCC Glove Composites

A desired content of dried Aox-NCCs was mixed with NBR latex and stirred vigorously at room temperature for 30 minutes before compounding. Then, the compounding of NBR/Aox-NCCs with other ingredients were carried out in a beaker with a continuous stirring process. The glove of NBR/Aox-NCC composites was prepared with the dipping tank method. The former used was made from ceramic. First, the clean former was dipped in coagulant and drying, after that the former with coagulant was dipped in latex then drying. After dried, the former with the latex was dipped in warm water to remove uncured excess latex and impurities. Then, the latex was rinsing and final drying before stripping. The process was illustrated in Figure 1. By changing the contents of NCCs over the range of 0 phr, 1 phr, 2 phr, 3 phr, 4 phr and 5 phr, a series of NBR composites with thickness around 8 mm were prepared and coded as NBR control, NBR/Aox -NCC 1 phr, NBR/Aox -NCC 2 phr, NBR/Aox

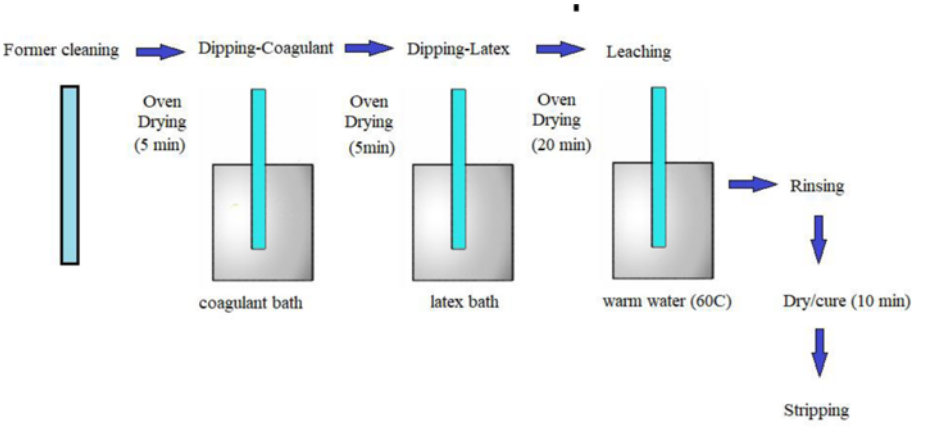

Figure 1. Dipping method process.

-NCC 3 phr, NBR/Aox -NCC 4 phr, and NBR/Aox -NCC 5 phr, respectively.

Cross-linking Density Test

Each sample was cut with dimension 10 mm×10 mm× 0.8 mm. The films were thin enough for diffusion was supposed to be unidirectional and allowed all parts of films were affected. The samples were transferred in bottles (immersed in 20 m*l* toluene) and went on in the dark to prevent oxidation and under room temperature condition. The samples were taken out from the bottles after 72 hours and blotted with a tissue to remove excess toluene, no press was added to the samples. The samples then were considered immediately. After that, the samples, then were kept in oven for 60 ^{o}C until 48 hours and then were counted again. The volume fraction of rubber in the gel, Vr was used to represent the cross linking density of the samples, the calculation was used as follows according to method describe by [20];

The volume fraction (Vr) was calculated according to the following equation as in equation (1):

$$\frac{1}{Vr} = 1 + \frac{m_s - m_u}{m_u} \cdot \frac{\rho_r}{\rho_s} \quad (1)$$

where m_s the mass of vulcanized NBR/NCC in swollen state is after equilibrium swelling in toluene, m_u is the mass of NBR/NCC in air.

The whole crosslink density, (*Ve*) was calculated by the Flory-Rehner equation as in equation (2)

$$Ve = \frac{\ln(1 - Vr) + Vr + \chi V_{r2}}{Vs(Vr^{1/3} - Vr/2)} \quad (2)$$

where *Vr* is the volume of fraction of the polymer swollen to equilibrium and V_s is the molar volume of solvent used (toluene=106.2 cm^2/mol), χ the polymer-solvent interaction parameter (NBR-toluene=0.435), ρ_r and ρ_s are the density of the rubber and toluene (ρ_r=1.17 g/cm^3; ρ_s=0.865 g/cm^3), respectively.

Fourier Transform Infra-Red (FTIR) Spectra Analysis

The FTIR spectra of NCC, standard gallic acid and Aox-NCC were measured with a Thermo Nicolet FTIR spectrometer (Nicolet 6700, USA) in a range of 4000-450 cm^{-1} at a resolution of 4 cm^{-1} and 32 scans were recorded per sample. Each sample was palletized with KBr powder to prepare pastille. For NBR and NBR composites, a small piece (1.0 cm×1.0 cm) was cut from the samples before analyzed by ATR method with same resolution and scan.

Magnetic Resonance (NMR) Analysis

The 1H NMR spectrums were determine by using a Brucker AV 400 spectrometer at 25 ^{o}C with a resonance frequency of 400 MHz. NCC and antioxidant NCC were dissolved in deuterated dimethyl sulphoxide (DMSO-d6). All analysis using NMR were carried out at room condition.

X-ray Diffractogram (XRD) Analysis

The XRD analysis was used to study the crystalline structural changes of the cellulose before and after gallic acid treatment. The samples data was determined by using X-ray diffractometer at 45 kV and 100 mA. The diffracted intensity of Cu Kα radiation (λ=0.1541 nm) was recorded in a 2θ range of 4-40 at a rate of 1 ^{o}/min with a resolution of 0.05 ^{o} and step time of 2.5 s.

The crystallinity index was calculated from diffraction intensity data using as equation (3):

$$CrI = \frac{I_{002} - I_{am}}{I_{002}} \times 100 \quad (3)$$

where I_{002} is the overall intensity of the peak at 2θ about 22 ^{o} and I_{am} is intensity of baseline at 2θ about 18 ^{o}.

Thermogravimetric Analysis (TGA)

The thermal stability of sample was studied with the TGA that was performed using a GA Q500 (TA instruments, USA). About 5 mg of samples were heated from 30 ºC to 600 ºC with a heating rate of 10 ^{o}C/min under a nitrogen atmosphere. The weight change was recorded as a function of the heating temperature.

Differential Scanning Calorimetry (DSC) Analysis

The DSC analysis was performed on a DSC-Q200 instrument under a nitrogen atmosphere at a heating rate of 10 ^{o}C/min^{-1} and flow rate 50 m*l*/min. About 2 mg of each sample were placed in hermetically sealed DSC crimp pans, which were tested over a range of 25 to 450 ^{o}C.

Transmission Electron Microscopic (TEM) Analysis

Drops of 0.001 % of NCC and Aox-NCC suspensions were deposited on glow-discharged carbon-coated TEM grids. The specimen were then negatively stained with 2 % uranyl acetate, prior to complete drying and observed using a Philips CM200 electron microscope operating at 200 kV. Images were recorded on Kodak SO163 films. Images were analyses by using the Soft Imaging Viewer software.

Mechanical Tests

The tensile test was carried out by using the universal testing machine (UTM). The samples were cut in dog bone shape size dimension as in Figure 2 by using die cutter. All experiments were carried out at room temperature with a cross head speed of 500 mm/min according to ASTM D412. Tear test was conducted according to ASTM D624.

Soil Burial Test

Soil burial test was done to investigate the degradation rate of NBR composites film in soil environment condition. The films (3×3) cm were cut form NBR composites, then

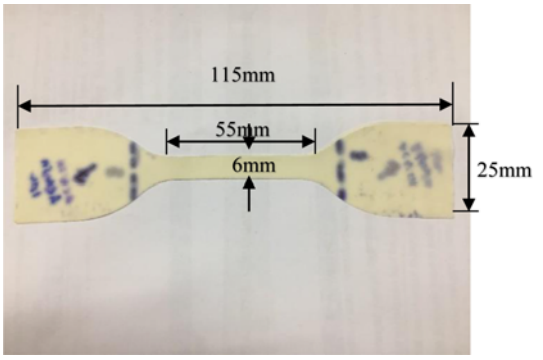

Figure 2. Size dimension for tensile test film (dog bone shape).

each pieces were buried vertically in nylon net mesh bags and transferred into a soil in plantation area (25 cm depth; pH 6.5-7; 28 °C to 30 °C) located at the Botanical Garden of University Malaya. Then, the film pieces were retrieved from soils after 8 weeks and 24 weeks, washed in running water and dried prior to weight. Percentage of weight loss was calculated by using equation (4):

$$\text{Weight loss } (\%) = \frac{W_i - W_a}{W_i} \times 100 \quad (4)$$

where W_i is the weight before soil burial test and W_a is the weight after soil burial test.

Field Emission Scanning Electron Microscopy (FESEM)

The smaller pieces (1.0 cm×1.0 cm) were cut before observation under FESEM. The surfaces of NBR/Aox-NCC composites were analysis by field emission scanning electron microscopic (FESEM) with voltage acceleration at 5 kV and low vacuum. Magnification at 10000x was used.

Results and Discussion

Crosslinking Density

Results in Figures 3 and 4 shows the volume fraction of rubber bonded and crosslinking density for NBR and NBR/ Aox composites with different Aox-NCCs loading. The increase of volume fraction and crosslinking densities was proportional with increment of Aox-NCCs content up until 3 phr then the values were dropped. In Figure 3 the value for control NBR was only 0.2585 whereas the NBR/Aox-NCC with 1 phr loading was 0.2667, NBR/Aox-NCC with 2 phr was 0.2807, NBR/Aox-NCC with 3 phr was 0.3069, NBR/ Aox-NCC with 4 phr was 0.2716 and NBR/Aox-NCC with 5 phr was 0.2725. It shows the highest was for NBR/Aox-NCC with 3 phr as compared to the control NBR. For 4 phr and 5 phr the values were slightly dropped due to entanglement of Aox-NCCs between each other. The dissolution of a limited amount of neat NBR was ascribed to the fact that experiment was form in the room temperature without any stirring. This condition was in line with previous study by

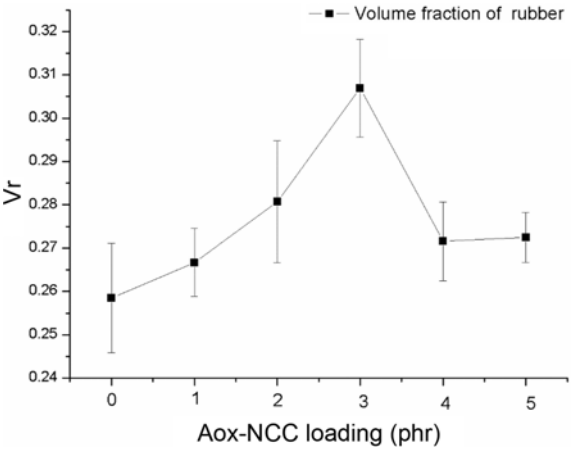

Figure 3. Volume fraction of rubber for NBR and NBR/NCC composites.

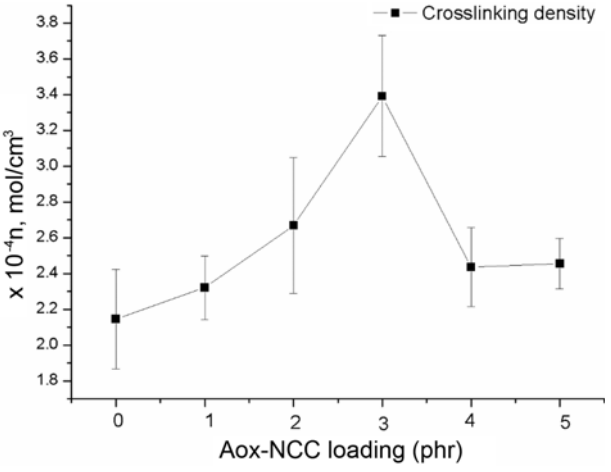

Figure 4. Cross-linking density for NBR and NBR/NCC composites.

[21] that stated only 13 % dissolution of rubber matrix in toluene. The bonded NBR matrix with Aox-NCCs was remaining in toluene medium. Other reason was due to formation of rigid Aox-NCCs network in the rubber matrix that involve the interfacial interaction between Aox-NCCs and matrix and prevent the dissolution of rubber chains and maintain in gel fraction of the sample. This behavior in line with increase the interfacial interactions between the NBR chains and NCCs surface, thus preventing the dissolution of the rubber matrix in toluene. A filler networks is formed with the addition of Aox-NCCs at certain value, which further restrict the mobility of NBR chains, thus improving the crosslink density of NBR/NCC composites (Figure 4). The results showed that NBR was 2.15×10^{-4}, NBR/NCC composite at 1 phr was 2.32×10^{-4}, NBR/NCC composite at 2 phr was 2.67×10^{-4}, NBR/NCC composite at 3 phr was 3.39×10^{-4}, NBR/NCC composite at 4 phr was 2.44×10^{-4} and NBR/NCC composite at 5 phr was 2.45×10^{-4} mol/cm^3.

Crosslink density is represent the microstructure of composites condition. It's demonstrate the condition of chemical crosslinks and physical absorption such as chain entanglements [22]. The increase of crosslinking density was in proportional with mechanical performance until up to 3 phr.

Fourier Transform Infra-Red (FTIR) Spectra Analysis

Figure 5 shows the FTIR spectra for NCC, standard gallic acid and Aox-NCC. Standard gallic acid was used as a reference. The NCC exhibited a broad peak at 3295 cm^{-1} due to stretching vibrations of O-H [23]. The peak at 2902 cm^{-1} was due to C-H stretching [24]. Peak at 1642 cm^{-1} was correspond to OH bending of absorbed moisture [25]. Peaks at 1151 cm^{-1} was assigned to asymmetric stretching of C-O-C bridge, 1054 cm^{-1} and 1028 cm^{-1} were corresponds to skeletal stretching of C-O [26]. The peak at 897 cm^{-1} was correspond for glycosidic bonds and designated for amorphous absorption that are related to COC, CCO and CCH deformation modes and stretching vibrations of the C-5 and C-6 atoms [27]. Wagging and twisting modes of anhydroglucopyranose unit are observed from 1800 to 600 cm^{-1} [1]. Characteristics of standard gallic acid was observed at peak 3409 cm^{-1} that was due to O-H stetching and at 1681 cm^{-1} for C-O stretching of COOH structure. The band at 1540 cm^{-1} and 1469 cm^{-1} are due to C-C aromatic ring stretching vibration. The peak at 868 cm^{-1} was reffered to C-H aromatic ring outside stretching with tetra replacement in 1, 3, 4, 5 which agreed with previous study by [28].

Significant peak was observed for Aox-NCC around 1700 cm^{-1}. This peak correspond to ester linkages between the NCC and gallic acid, respectively [29]. COOH group in gallic acid was converting to ester to facilitate reaction with NCC. The present of peak 3332 cm^{-1} indicated the existent of phenolic groups. A sharp peak at 3289 cm^{-1} that was detected in Aox-NCC corresponds to O-H group. The peak at 1694 cm^{-1} due to C-O stretching of carboxylic acid. A peak around 1600-1450 cm^{-1} was corresponds to the C=C stretching aromatic ring of gallic acid [29]. The bands at 1541 cm^{-1} and 1470 cm^{-1} are due to CC aromatic ring stretching vibration. The peaks at 1616 cm^{-1}, 1204 cm^{-1} and 1028 cm^{-1} were assigned to the C=O, C-O and O-H respectively. These peaks indicated the existent of gallic acid in Aox-NCC.

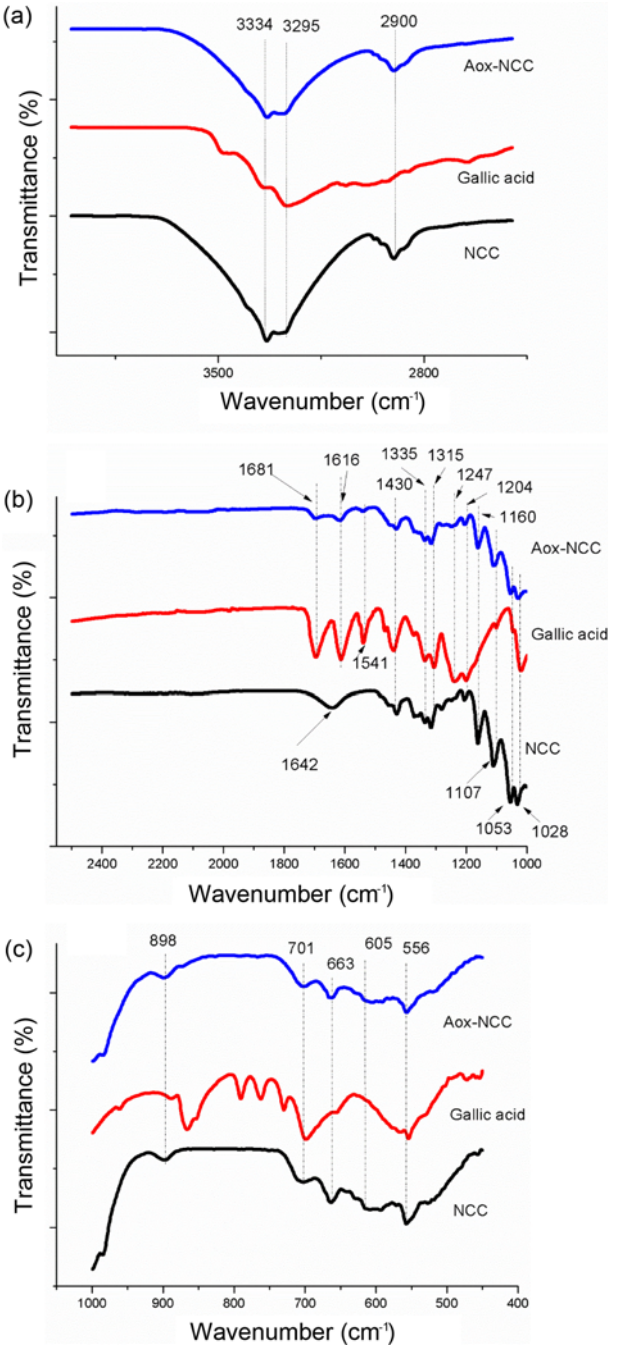

Figure 5. FTIR analysis for NCC, Gallic acid and Aox-NCC; (a) 4000-2500 cm^{-1}, (b) 2499-1000 cm^{-1}, and (c) 999-450 cm^{-1}.

Nuclear Magnetic Resonance (NMR) Analysis

The NMR spectra of NCC and Aox-NCC are presented in Figures 6(a) and 6(b), respectively. The NCC spectra shows the characteristic of protons of glucose units appeared at 4.68, 3.78, 3.56 and 3.07 ppm which belong to H-1, H-3,6,5, H-2 and H-4 in anhydrous glucose units (AGU) of cellulose, respectively. Meanwhile, the signals at 5.40 and 4.33 ppm were described to the H-3 and H-6 protons of residual hydroxyl in cellulosic compounds. In Figure 6(b), the ^{1}H NMR spectra for Aox-NCC showed the abundant peaks at region 1.50 to 3.50 ppm are corresponding to C_2H_4 groups of cyclic ring of AGU. Meanwhile, weak signal peak at 4.28 ppm belongs to C_2H_4 proton, H-6 attached to ester groups. The weak signal of this proton was due to steric hindrance and highly electron density effects from adjacent aromatic rings. These effect make the methylene proton, H-6 signal of Aox-NCC becomes lower than methylene proton,

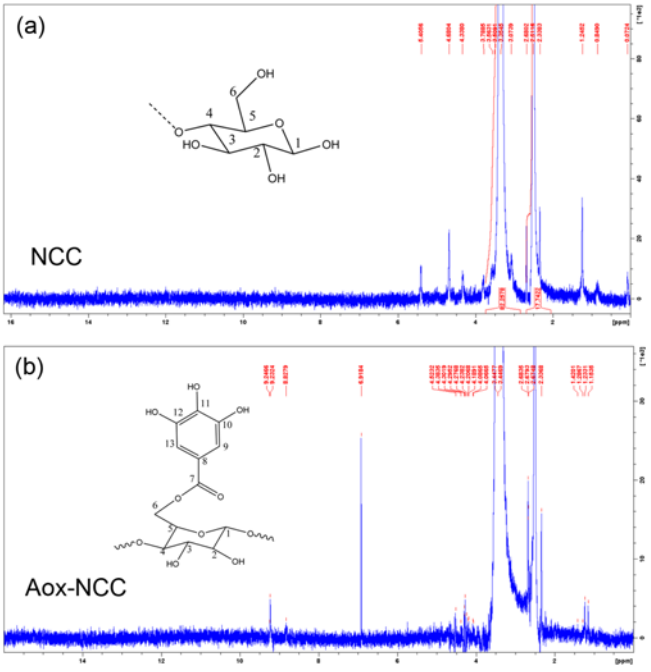

Figure 6. (a) NMR of NCC (0-16 ppm) and (b) NMR of Aox-NCC (0-16 ppm).

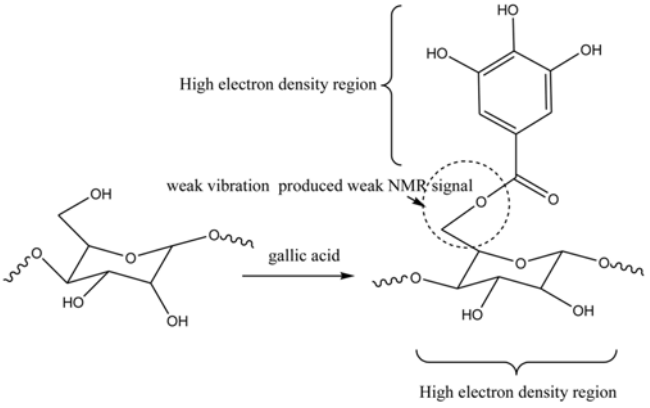

Figure 7. Reaction scheme of gallic acid on NCC.

H-6 of NCC. The presence of OH groups of Aox-NCC was observed at region 6.5 to 9.5 ppm. As in line with previous work by [28] indicate that the signal of hydroxyl in upper spectra mostly between region 9 to 11 ppm. This confirmed the successful attachment of gallic acid onto NCC by the comparison of NCC and Aox-NCC NMR spectra. Figure 7 show the reaction scheme of gallic acid attachment on NCC backbone.

X-ray Diffraction (XRD) Analysis

The phase characteristic of sample is studied by XRD analysis and it was recorded as 59.14 % and 71.45 % for the NCC and Aox-NCC, respectively (Figure 8, Table 1). This indicated that the NCC treated with Gallic acid had higher

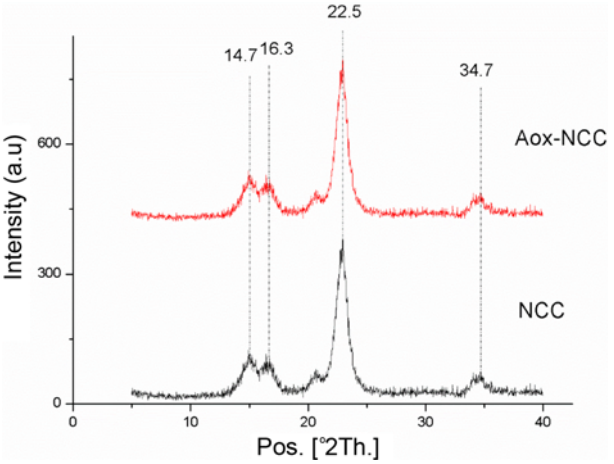

Figure 8. XRD of NCC and Aox-NCC.

Table 1. Crystallinity index (CrI) of antioxidant NCC and Aox-NCC

Sample	CrI (%)
NCC	59.14
Aox-NCC	71.45

crystallinity than unmodified NCC due to removing of amorphous part on NCC during modification process. Both of samples showed the cellulose I characteristic peaks at 2θ= 14.7 ° (101), 16.3 (10Ĺ), and 22.5 ° (002) and 34.7 (040) [1, 30]. The peak intensity of the (002) plane (2θ=22.5 °) in the diffraction increased slightly for Aox-NCC sample indicating that higher perfection of crystal lattice [1] as well as the crystallinity index. The peak of 2θ=14.7 become more intense and separated from peak 2θ=16.3 indicating that a more compact and ordered arrangement.

Thermogravimetric Analysis (TGA)

The thermal properties of NCC and Aox-NCC was studied in details by TGA and DTG as in Figure 9(a) and Figure 9(b). As shown in Figure 9(a) the TGA curves NCC and Aox-NCC curves are very similar, which can be distinctly divided into three stages: During initial stage from room temperature to 100 °C, the water and other residue solvent vaporized. Weight loss below 100 °C was attributed to water and moisture content. The Aox-NCC result in greater amount of weight loss than NCC due to more water content and moisture capacity on Aox-NCC than NCC. Both of the NCC and Aox-NCC have hydrophilic properties that have tendency to absorb moisture/water. The degradation patterns are identical for all samples. The dominant peak between 300 °C and 350 °C was a result from concurrent degradation process such as depolymerization, dehydration, decomposition of the glycosyl rings and destruction of crystalline part occurred, then subsequent formation of charred residues

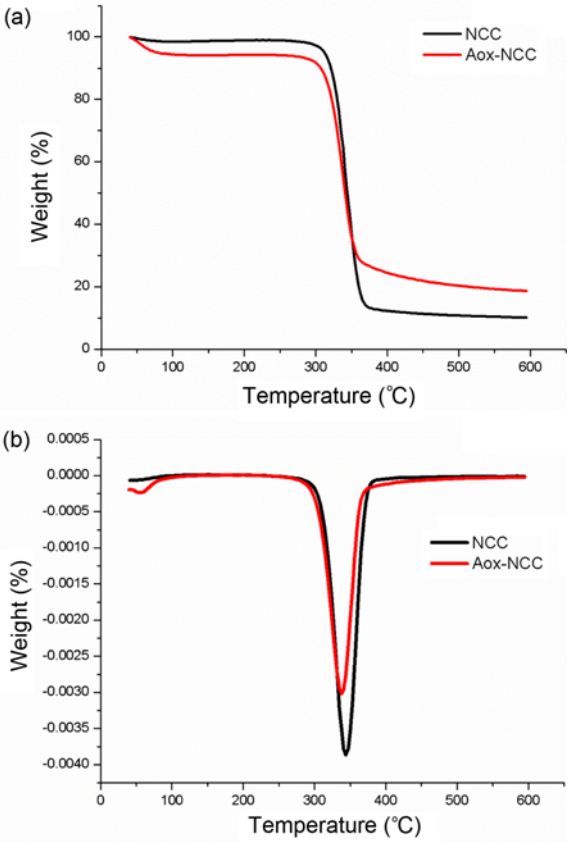

Figure 9. (a) TGA of NCC and Aox-NCC and (b) DTG of NCC and Aox-NCC.

[31]. The peak above 350 °C was due to the oxidation and breakdown of the charred residue into gaseous products with low molecular weight, the crystalline part was completely decompose into monomer chain of D-glucopyranose [32]. Based on the result the onset temperature for NCC is 324.27 °C whereas onset temperature for Aox-NCC is 317.25 °C. This indicate that less activation energy is required to start thermal degradation for Aox-NCC. Higher surface area of particles might also contributed to more exposure surface area to heat, thus diminishing their thermo stability. The char residues for NCC is 10.06 % and for Aox-NCC is 18.60 %. The increase of char residue in Aox-NCC due to the present of COOH groups.

Differential Scanning Calorimetry (DSC) Analysis

Figure 10 shows the DSC of NCC and Aox-NCC with two different endotherms thermos-event. The first endotherm of occurred between temperature range of 34 °C to 109 °C for NCC and Aox-NCC was in range of 36 °C to 118 °C. Within both range of endotherms, both samples indicated evaporation of moisture or low molecular weight component coupled with glass transition. This report was in line with previous report by [33] that investigated the loss of moisture with

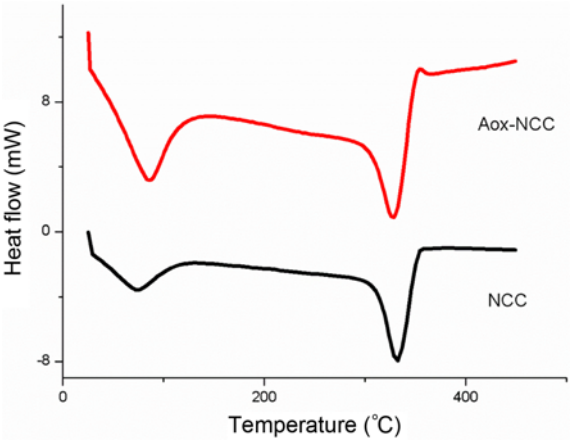

Figure 10. DSC of NCC and Aox-NCC.

glass temperature within the same range on gallic acid cellulose acetate. Furthermore, it was found that the endothermic peak area within this range of Aox-NCC was larger than NCC that could be resulted by incorporated of gallic acid on NCC increased the moisture absorption. Second endotherms transition was occurred between temperature of 310 °C to 351 °C for NCC and 306 °C to 348 °C for Aox-NCC. This region of endotherms transition was attributed to the crystalline part. The melting of glucosidic bonds between NCC and depolymerization of cellulose chains were occurred in this region as indicated by [34]. A sharp endothermic in these regions were resulted from fusion of crystalline part with the peak sharp of NCC was 331 °C and Aox-NCC was 328 °C. The decrease of the peak temperature on this region could be due to increase of amorphous part and reduction in cellulose crystallite size [35].

Transmission Electron Microscopic (TEM) Analysis

Figures 11(a) and 11(b) shows the TEM image of NCC and Aox-NCC samples. As in Figure 11(a) shows that the NCC structure was in spherical or spheres shape, with the agglomeration, sticking and embedded together. The TEM images of NCC and Aox-NCC showed width and length was

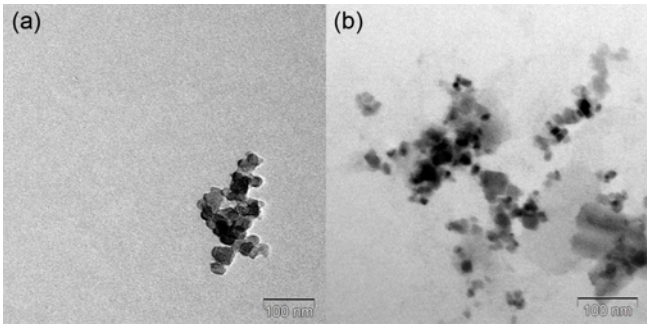

Figure 11. TEM of (a) agglomerated NCC and (b) scattered Aox-NCC.

less than 100 nm (Figures 11(a) and 11(b)). It was found that aggregation of Aox-NCC did occurs to form larger chain bundle as for NCC. The extended network for Aox-NCC could be due also from the less dispersed Aox-NCC in water. The NCC was embedded together in abundant spherical cellulose. However, these agglomerated bundles were in the loosely packed structure. Both of NCC and Aox-NCC were in spherical or spheres form. The self-assembled was due to interfacial hydrogen bonds and/or during process involved in preparing the Aox-NCC treatment. Both of NCC and gallic acid component was hydrophilic in properties which abundantly perform of inter hydrogen bonds within the OH groups.

Mechanical Test

Figure 12 and Table 2 show the mechanical performance for NBR and NBR/Aox-NCC composites. The tensile strength of the Aox-NCC NBR composites was increases from 1 phr to 3 phr compared to control NBR then started to significantly drop for 4 phr until 5 phr. The reason is due to effective crosslinking of Aox-NCC to NBR chains up to 3 phr. On top of that, the inhomogeneous dispersion of Aox-NCC within the NBR matrix brought to the significant reduction on tensile strength at 4 and 5 phr of filler loading. This was in agreement with another study by [36,37]. A good interfacial bonding between filler and polymer matrix resulted in better stress transfer. Modulus at 100 % strain showed insignificant improvement with addition of the Aox-NCC compared to control NBR. Modulus at 300 % strain gave a slight improvement on NBR composites start from 1 phr that was 1.39 MPa, 2 phr was 1.45 MPa, 3 phr was 1.67 MPa and then no significant improvement for addition to 4 phr and 5 phr that were 1.35 MPa and 1.48 MPa as compared with neat NBR (1.35 MPa). Modulus at 500 % strain showed the significant improvement with the addition of Aox-NCC to NBR composites with control NBR was 1.68 MPa, 1 phr was 1.94 MPa, 2 phr was 2.10 MPa, 3 phr was 2.42 MPa, 4 phr was 1.90 MPa and 5 phr was 2.01 MPa, however the improvement until 3 phr then demonstrate some reduction from 4 phr to 5 phr due to the effective crosslinking between Aox-NCCs and NBR chains only. Table 3 also showed the elongation at break that only gave some improvement on composites, addition of Aox-NCC form some agglomeration spot on NBR surface thus lowering the elongation at break value. The presence of NCC contents and inactive surface of fillers would affect the dispersion and agglomeration in composites [38]. Tear strength was reduced and no significant improvement was observed with addition of Aox-NCC in NBR matrix with control NBR was 15.01 kN/m, 1 phr was 12.42 kN/m, 2 phr was 11.43 kN/m, 3 phr was 13.37 kN/m, 4 phr was 14.66 kN/m and 5 phr was 14.59 kN/m. Formation of more hydrogen bonding between the Aox-NCCs could form the tendency to create spotted on NBR composites thus not assist in stopping the tear force when the tearing effect. The tensile strength and Modulus were improved steadily up to 3 phr and started to drop at 4 phr and 5 phr, the elongation at break was decreased, the increase in tensile strength was due to the restriction of polymer chain mobility in the vicinity of Aox-NCC particles. The elongation at break was decrease with the increase of phr content due to strong network was formed between NBR chains and strong interaction between NBR and Aox-NCC, which decreased the ability to resist deformation of rubber chains [22].

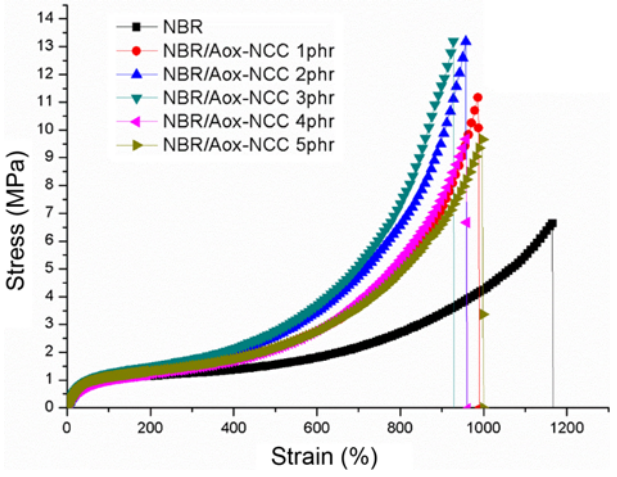

Figure 12. Stress-strain curve for NBR and NBR/Aox-NCC composites.

Table 2. Mechanical properties of antioxidant NCC reinforced NBR glove composites

NCCs content (phr)	Tensile strength (MPa)	Modulus at 100 % strain (MPa)	Modulus at 300 % strain (MPa)	Modulus at 500 % strain (MPa)	Elongation at break (%)	Tear strength (kN/m)
0	8.26 (1.07)	1.06 (0.18)	1.35 (0.28)	1.68 (0.48)	3.46 (0.65)	15.01 (1.85)
1	8.69 (1.74)	1.01 (0.02)	1.39 (0.04)	1.94 (0.07)	3.46 (0.07)	12.42 (1.47)
2	9.52 (1.70)	1.04 (0.46)	1.45 (0.09)	2.10 (0.18)	3.50 (0.15)	11.43 (0.83)
3	11.86 (1.32)	1.19 (0.02)	1.67 (0.02)	2.42 (0.03)	4.20 (0.07)	13.37 (0.85)
4	7.32 (0.38)	0.97 (0.03)	1.35 (0.08)	1.90 (0.15)	3.54 (0.14)	14.66 (0.99)
5	8.85 (1.16)	1.09 (0.04)	1.48 (0.04)	2.01 (0.04)	4.01 (0.23)	14.59 (1.03)

*Standard deviations are shown in brackets.

Table 3. Biodegradation of NBR and Aox-NCC/NBR composites

Sample type	2 month (% weight)	6 month (% weight)
NBR control	10.103 (2.34)	12.413 (0.33)
Aox-NCC/NBR composite 1 phr	11.010 (1.18)	11.270 (0.93)
Aox-NCC/NBR composite 2 phr	9.544 (1.41)	9.153 (0.95)
Aox-NCC/NBR composite 3 phr	11.836 (1.89)	11.959 (0.51)
Aox-NCC/NBR composite 4 phr	9.837 (1.52)	11.609 (1.56)
Aox-NCC/NBR composite 5 phr	12.749 (1.83)	15.031 (1.78)

*Standard deviations are shown in brackets.

Soil Burial Test

Table 3 show the bio-degradability profile of control NBR and NBR/Aox-NCC composite films during soil buried process for the 2 and 6 months period. There was no significant changes on the weight between the neat NBR and NBR/Aox-NCC composites from 1 phr to 5 phr, due to the slow rate degradation process. During this period, the degradation process performed on the synthetic NBR region as compared to filled region. Aox-NCCs in NBR/Aox-NCC composite films also was recorded with no significant degradation process within 2 months as compared in 6 months period. It is believe that, modification of the NCC by gallic acid increase the resistance of composites degradation in soil medium. This is in agreement with the previous report highlights that the modification of filler reduces the degradation rate of composites [39]. The Aox-NCC degradability was started to degraded within half year in soil environment. Continuation of this study a complete degradation process of the composites is expected to take longer duration. In glove manufacturing, antioxidants are used as an ageing protectors of rubber compounding. The antioxidant act as chain breaking donors when added to polymeric materials to remove the alkyl (P-) or alkylperoxy radicals (POO-) during oxo-biodegradation by reduction to hydro peroxides (ROOH) [6]. Increase addition of Aox-NCC in NBR matrix was scattered that resulted in non-uniformity or homogenous tabulated in NBR matrix, this are the reason the rate degradation of the NBR/Aox-NCC composite at 2 phr and NBR/Aox-NCC composite at 4 phr samples was lower than other samples.

Chemical Composition Analysis by FTIR on NBR/Aox-NCC Composites

FTIR was used to analyze the chemical composition changed after and before the soil burial test was conducted. The result for neat NBR and NBR/Aox-NCC composites were presented in Figure 13. The peak at 2919 cm^{-1} and 2849 cm^{-1} were aassigned to stretching vibration of -CH_2

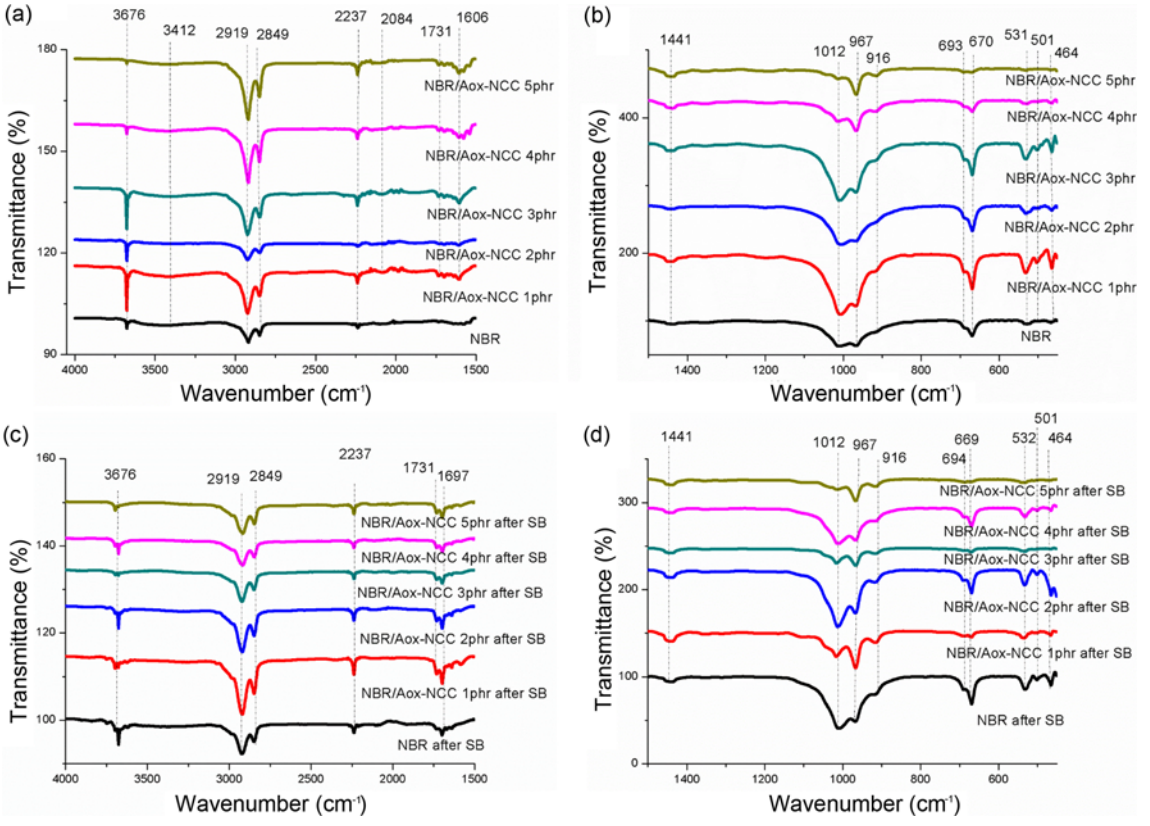

Figure 13. Analysis on chemical composition by FTIR before soil burial (SB) test; (a) 4000-1500 cm^{-1}, (b) 1499-450 cm^{-1} and after soil burial (SB) test, (c) 4000-1500 cm^{-1}, and (d) 1499-450 cm^{-1}.

[40]. The peak at 1441 cm^{-1} was contributed by bending vibration of -CH_2 [20]. The peak at 2237 cm^{-1} was originally come from nitrile stretching vibration [41]. Peak 967 cm^{-1} also was from C-H stretching vibration of butadiene double bond [41]. Broad peak around 3412 cm^{-1} was gone after SB followed by prominent peak at 1731 cm^{-1} and 1697 cm^{-1} that were contributed to carbonyl groups [42] was observed after SB. The peak 1606 cm^{-1} that was due to aromatic C=C vibrations [43] in Aox-NCC was diminished after SB and then was followed by changed and reduction in peak around 1012 cm^{-1} that was attributed to unsymmetrical C-O-C bond and C-O bond of primary alcohol [44] that was found also in Aox-NCC and changes in NBR/Aox-NCC composite peaks at 967 cm^{-1} were observed after SB and also the reduction and shifted in peak 670 cm^{-1} to 669 cm^{-1} that was assigned to aromatic C-C stretching [40] after SB.

Field Emission Scanning Electron Microscopy (FESEM) Analysis

Figures 14(a) to 14(f) show the morphology of control

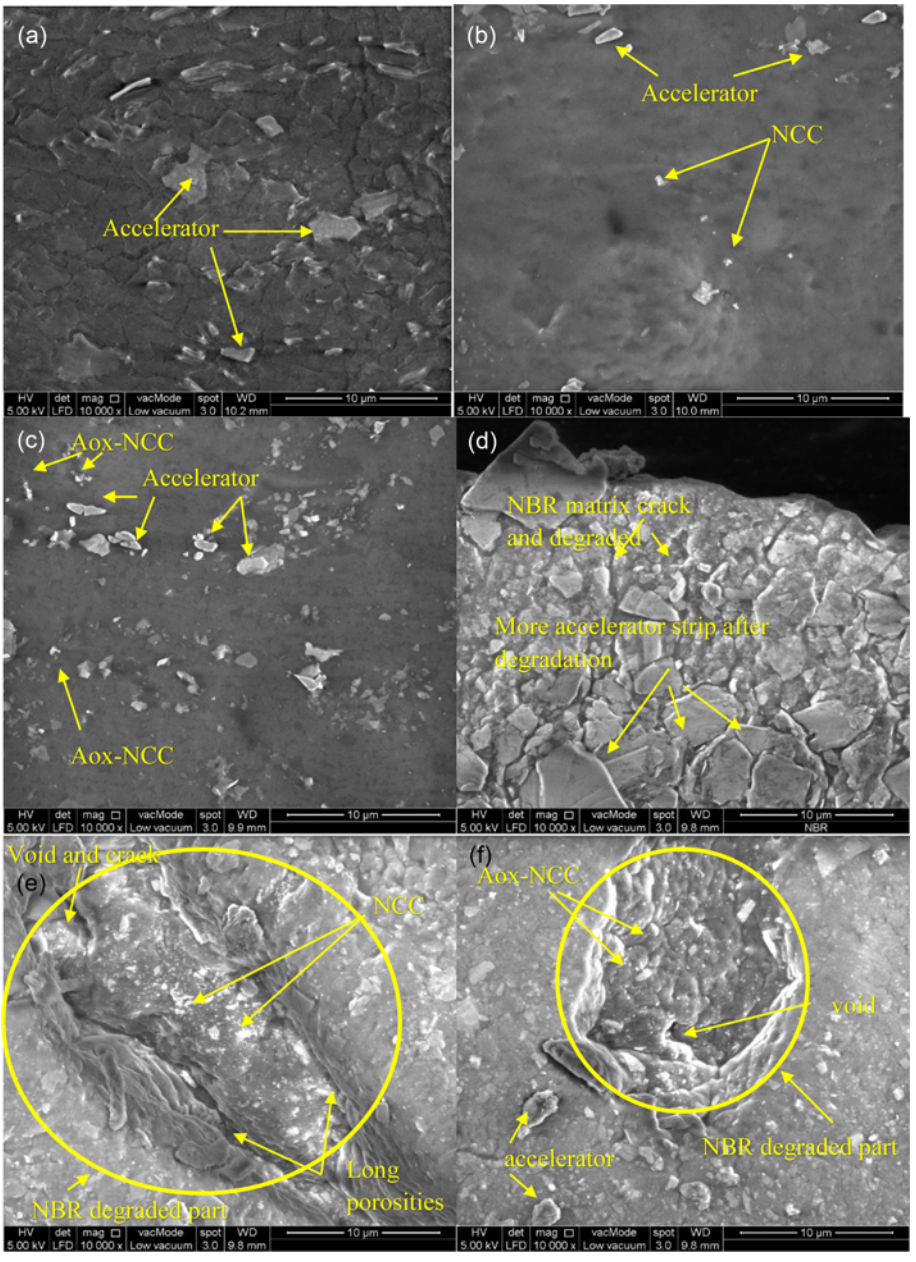

Figure 14. (a) FESEM images of NBR control before soil burial test, (b) Aox-NCC/NBR composites at 1 phr before soil burial test, (c) Aox-NCC/NBR composites at 5 phr before soil burial test, (c) NBR control after 6 months soil burial test, (d) Aox-NCC/NBR composites at 1 phr after 6 months soil burial test, and (e) Aox-NCC/NBR composites at 5 phr after 6 months soil burial test.

NBR and NBR/Aox-NCC composites at 1 phr and 5 phr before and after the soil burial test. Figures 14(a) demonstrate that the control NBR showed the clean, neat with the accelerator on the surface whereas, Figures 14(b) and (c) NBR/Aox-NCC composites showed the scattered of Aox-NCC as can be identified as white dots on the surface of NBR matrix. Continuous addition of Aox-NCC into NBR composites showed the Aox-NCC start to agglomerated and located as spotted on the NBR composites due to effect of hydrogen bonding as in Figure 14(c)). Brittleness also occurred when the excess Aox-NCC was added into the matrix as shown in Figure 14(c).

Figures 14(d) to 14(f) show the morphology on surface and structure of control NBR, NBR/Aox-NCC composites at 1 phr and NBR/Aox-NCC composites at 5 phr after 6 month soil burial test was conducted. From the Figures 14(d) to 14(f) showed that the cracks and voids were observed for overall of samples. Control NBR sample (Figure 14(d)) after 6 month soil burial, showed some voids and cracks were observed and the accelerator still be detected and observed on the composite surfaces, this mean that accelerator not degraded in the soil due to properties of accelerator are come from inorganic materials. The finding is supported with previous report mention on the degradation rate is reducing with the presence of non-biodegradable materials. This was in agreement with study by [45]. As can be seen on Figures 14(e) and 14(f) showed that the cracks and voids with the big cavities also was observed for 1 phr to 5 phr. This is attributed to the removing of some part on NBR/Aox-NCC composites, this could be due to degradation of Aox-NCC component. Aox-NCC was bio-degradable and come from organic materials. The hydrophilic properties in nature of Aox-NCC may alter the degradation rate of composite due to high hygroscopicity [46]. The Aox-NCC breakdown of cellulose glycosidic linkage resulted from microorganism cleavage. Degradation of Aox-NCC component in the composites lead to formation of voids, porosities and loss of integration of NBR matrix as can be seen in FESEM results. Some of Aox-NCCs were remains on the surface after 6 month in the soil, this can explain that the Aox-NCC not fully degraded in the soil and longer time is needed to complete the degradation. It is clear that, the NBR matrix degraded slowly with relatively low weight loss, the addition of Aox-NCC in NBR composites slowly increase or slowly accelerates the rate of biodegradation on NBR composites. As reported by Zhou *et al.* [47] biodegradation of rubber nano composites was commonly took place in soil or compost, then the material decomposed into water and CO_2 by biological activities that changes the chemical structures of materials.

Conclusion

The NCC was successfully modified with gallic acid as antioxidant moiety to produce Aox-NCC. Then, the Aox-NCC has been applied as reinforcement in NBR matrix. Results from FTIR, NMR. XRD, TGA, and TEM demonstrated that the gallic acid moiety has been successfully modified the surface functionality of NCC by formation of carboxylate linkage. Meanwhile, XRD result showed higher crystallinity index exhibited for Aox-NCC compared with NCC. Morphological images from TEM analysis shown the agglomeration was performed between Aox-NCC nanoparticles due to the abundant number of hydrogen bonding The mechanical properties exhibited for NBR/Aox-NCC composites was improved up to 3 phr then started to drop, no significant improvement for the modulus at 100 % and modulus at 300 %, significant improvement on modulus was observed only at 500 % and no significant result for elongation at break. Tear strength also showed slight improvement with addition of Aox-NCC in the NBR matrix. For soil burial test, degradation process took much longer period to degrade within 2 months period no significant result was obtained for NBR/Aox-NCC composite films as compared within 6 months period. The degradation of NBR/Aox-NCC composites were accompanied by the changes in chemical composition as in FTIR results. As can be seen on FESEM, addition of more Aox-NCC in NBR matrix created agglomeration due to rich hydroxyl groups between Aox-NCCs and tend to degrade and leave the large voids and porosities on the NBR composites surface.

Acknowledgements

The authors would like to thank to University of Malaya for providing financial support on this project. This project was financially supported by Postgraduate Research Grant (PPP) (PG238-2015A: Effects on surface acetylated nanocrystalline cellulose (NCC) reinforced in nitrile butadiene rubber (NBR) composite). Special thanks to Nanotechnology and Catalysis Research Centre (NANOCAT) for laboratory facilities.

References

1. P. Lu and Y.-L. Hsieh, *Carbohydr. Polym.*, **82**, 329 (2010).
2. X. Wang, P. Qu, and L. Zhang, *Fiber. Polym.,* **15**, 302 (2014).
3. A. L. S. Pereira, D. M. do Nascirnento, M. D. M. Souza, J. P. S. Moraisd, N. F. Vasconcelos, J. P. A. Feitosa, A. I. S. Brigida, and M. D. Rosa, *Carbohydr. Polym.*, **112**, 165 (2014).
4. J. Araki, *Soft Mater.,* **9**, 4125 (2013).
5. K.-Y. Lee, Y. Aitomäki, L. A. Berglund, K. Oksman, and A. Bismarck, *Compos. Sci. Technol.*, **105**, 15 (2014).
6. L. V. Abad, L. S. Relleve, C. T. Aranilla, A. K. Aliganga, C. M. San Diego, and A. M. dela Rosa, *Polym. Degrad. Stabil.*, **76**, 275 (2002).

7. K. M. Z. Hossain, N. Sharif, N. Dafader, M. Haque, and A. Chowdhury, *ISRN Polym. Sci.*, **2013** (2013).
8. A. Ikram, M. Ma Azam, M. Amir Hashim, M. Fauzi, A. Shamsul Bahri, and S. Kamaruzaman, *J. Rubber Res.*, **8**, 220 (2005).
9. R. N. Phalen, T. Le, and W. K. Wong, *J. Occup. Environ. Hyg.*, **11**, 716 (2014).
10. M. M. Aliabadi, G. Naderi, S. J. Shahtaheri, A. R. Forushani, I. Mohammadfam, and M. Jahangiri, *Iran. Polym. J.,* **23**, 289 (2014).
11. Z. Wei, Y. L. Lu, Y. Meng, and L. Q. Zhang, *J. Appl. Polym. Sci.*, **124**, 4564 (2012).
12. Y. K. Chen, C. H. Xu, and Y. P. Wang, *J. Reinf. Plast. Compos.*, **31**, 705 (2012).
13. C. Sirisinha and N. Prayoonchatphan, *Plast. Rubber Compos.*, **30**, 24 (2001).
14. M. M. Salehi, T. Khalkhali, and A. A. Davoodi, *Polym. Sci. Ser. A*, **58**, 567 (2016).
15. V. K. Singh, A. Shukla, M. K. Patra, L. Saini, R. K. Jani, S. R. Vadera, and N. Kumar, *Carbon*, **50**, 2202 (2012).
16. D. E. El-Nashar and E. M. Sadek, *High Perform. Polym.*, **24**, 664 (2012).
17. A. Mohamed, T. Ardyani, S. A. Bakar, P. Brown, M. Hollamby, M. Sagisaka, and J. Eastoe, *Adv. Colloid Interface Sci.*, **230**, 54 (2016).
18. L. D. Perez, M. A. Zuluaga, T. Kyu, J. E. Mark, and B. L. Lopez, *Polym. Eng. Sci.*, **49**, 866 (2009).
19. P. A. Carson, "Hazardous Chemicals Handbook", Butterworth-Heinemann, 2002.
20. X. Ge, M. C. Li, X. X. Li, and U. R. Cho, *Appl. Clay Sci.*, **118**, 265 (2015).
21. M. Liu, Q. Peng, B. Luo, and C. Zhou, *Eur. Polym. J.*, **68**, 190 (2015).
22. X. Cao, C. Xu, Y. Wang, Y. Liu, Y. Liu, and Y. Chen, *Polym. Test.*, **32**, 819 (2013).
23. I. Shahabi-Ghahafarrokhi, F. Khodaiyan, M. Mousavi, and H. Yousefi, *Fiber. Polym.,* **16**, 529 (2015).
24. W. T. Wulandari, A. Rochliadi, and I. M. Arcana, *IOP Conf. Ser. Mater. Sci.*, **107**, 012045 (2016).
25. X. Luo and X. Wang, *BioResources*, **12**, 5826 (2017).
26. M. R. K. Sofla, R. J. Brown, T. Tsuzuki, and T. J. Rainey, *Adv. Nat. Sci.-Nanosci Nanotechnol.*, **7**, 035004 (2016).
27. S. Y. Oh, D. I. Yoo, Y. Shin, and G. Seo, *Carbohydr. Res.*, **340**, 417 (2005).
28. A. de Cristo Soares Alves, R. M. Mainardes, and N. M. Khalil, *Mater. Sci. Eng. C-Mater. Biol. Appl.,* **60**, 126 (2016).
29. S.-D. Yoon, Y.-M. Kim, B. I. Kim, and J.-Y. Je, *J. Photochem. Photobiol. B-Biol.*, **176**, 145 (2017).
30. A. El Oudiani, Y. Chaabouni, S. Msahli, and F. Sakli, *Carbohydr. Polym.*, **86**, 1221 (2011).
31. N. Wang, E. Ding, and R. Cheng, *Polymer*, **48**, 3486 (2007).
32. T. Fattahi Meyabadi, F. Dadashian, G. Mir Mohamad Sadeghi, and H. Ebrahimi Zanjani Asl, *Powder Technol.*, **261**, 232 (2014).
33. D. Singh, M. Singh Maniyari Rawat, A. Semalty, and M. Semalty, *Lett. Drug Des. Discov.*, **8**, 284 (2011).
34. L. C. Yeng, M. U. Wahit, and N. Othman, *J. Teknol.*, **75**, 107 (2015).
35. J. I. Morán, V. A. Alvarez, V. P. Cyras, and A. Vázquez, *Cellulose*, **15**, 149 (2008).
36. M. Przybyłek, M. Bakar, M. Mendrycka, U. Kosikowska, A. Malm, M. Worzakowska, T. Szymborski, and K. Kędra-Królik, *Mater. Sci. Eng. C-Mater. Biol. Appl.,* **76**, 269 (2017).
37. W. J. Chen, J. Gu, and S. H. Xu, *Express Polym. Lett.,* **8**, 659 (2014).
38. V. Baheti, R. Mishra, J. Militky, and B. K. Behera, *Fiber. Polym.,* **15**, 1500 (2014).
39. C. Sareena, M. Sreejith, M. Ramesan, and E. Purushothaman, *J. Reinf. Plast. Compos.,* **33**, 412 (2014).
40. D. A. Baeta, J. A. Zattera, M. G. Oliveira, and P. J. Oliveira, *Braz. J. Chem. Eng.*, **26**, 23 (2009).
41. S. Rajesh Kumar, P. M. Asseref, J. Dhanasekaran, and S. K. Mohan, *RSC Adv.*, **4**, 12526 (2014).
42. M. M. Hassan, R. O. Aly, A. El-Ghandour, and H. A. Abdelnaby, *J. Elastomer Plast.,* **45**, 77 (2013).
43. L. M. Wu, D. S. Tong, L. Z. Zhao, W. H. Yu, C. H. Zhou, and H. Wang, *Appl. Clay Sci.*, **95**, 74 (2014).
44. M. H. Izmar, M. M. Afiq, and A. R. Azura, *Compos. Pt. B-Eng.*, **43**, 2746 (2012).
45. T. W. Cho and S. W. Kim, *J. Appl. Polym. Sci.,* **121**, 1622 (2011).
46. M. Musioł, H. Janeczek, S. Jurczyk, I. Kwiecień, M. Sobota, A. Marcinkowski, and J. Rydz, *Fiber. Polym.,* **16**, 1362 (2015).
47. Y. Zhou, M. Fan, L. Chen, and J. Zhuang, *Compos. Pt. B-Eng.*, **76**, 180 (2015).